Doubly excited autoionizing states of H_2 converging to the $H(n=2)+H(n'=2)$ limit

Yulian V. Vanne and Alejandro Saenz
AG Moderne Optik, Institut für Physik, Humboldt-Universität zu Berlin, Hausvogteiplatz 5-7, D-10117 Berlin, Germany

Alex Dalgarno
Institute for Theoretical Atomic and Molecular Physics, Harvard-Smithsonian Center for Astrophysics, 60 Garden Street, Cambridge, Massachusetts 02138, USA

Robert C. Forrey
Penn State University, Berks-Lehigh Valley College, Reading, Pennsylvania 19610-6009, USA

Piotr Froelich
Department of Quantum Chemistry, Uppsala University, Box 518, S-75120 Uppsala, Sweden

Svante Jonsell
Theoretical Physics, Department of Physics, Umeå University, S-90187 Umeå, Sweden

(Received 16 November 2006; revised manuscript received 21 February 2006; published 7 June 2006)

A numerical investigation of the doubly excited states of H_2 converging to the $H(n=2)+H(n'=2)$ limit was performed. Special emphasis was put on the accurate description of the range of intermediate internuclear distances in order to correctly connect the short range with the asymptotic van der Waals regime where perturbation theory is applicable. The present nonperturbative calculation extends to internuclear separations $R=200a_0$ and is sufficiently accurate to achieve a connection between the two extreme regimes without any need for an interpolation procedure. The high precision of the *ab initio* results revealed a long range dipole-quadrupole interaction that had been omitted in two earlier calculations. In addition to revised first-order perturbation theory results the leading second-order term varying as R^{-6} was obtained. The impact of the present findings for cold $H(n=2)$ collisions is briefly discussed.

DOI: 10.1103/PhysRevA.73.062706 PACS number(s): 34.20.−b, 31.25.−v

I. INTRODUCTION

Doubly excited resonance states of H_2 contribute to the dissociative recombination of H_2^+ [1,2] and are responsible for structures in the kinetic energy distribution of protons produced in its dissociative ionization [3]. The so-called $Q(2)$ states separate at large internuclear distances R into a product of two hydrogen atoms each in a state with principal quantum number $n=2$. The mutual destruction of the $2s$ atoms in collisions limits the density of metastable atoms that can be achieved. This process may also be important in the interpretation of precision measurements of the two-photon transition frequency [4]. The excitation transfer reaction

$$H(2s) + H(2s) \rightarrow H(2p) + H(2p)$$

is followed by the emission of Lyman alpha photons and may be relevant to the production of a Lyman-α laser. Theoretical [5] and experimental [6] studies of the collision of two $H(2s)$ atoms have been carried out. There are small but significant discrepancies that may be related to the potential energy curves adopted.

In calculating the interaction potentials, three regions of R may be distinguished. The molecular region corresponds to small values of R where overlap and exchange forces play the major role. Variational methods may be used but here they must be modified to take into account that the states are resonance states that may undergo autoionization and decay [7]. Thus the interaction potentials are complex functions of R with imaginary parts. Previous calculations have used the R-matrix method [8], the complex scaling method [9] or the Feshbach projection technique, with Gaussian functions centered at the two nuclei [10] or with single center B-spline basis sets [11]. At large distances, electron exchange and overlap may be neglected, the interaction is weak and perturbation theory may be adopted. It leads to the representation of the interaction potential as a multipole expansion in powers of R^{-1}. The numerical demands on calculations at short and intermediate nuclear separations are severe, if a smooth matching of the potentials at short, intermediate, and long range is to be achieved.

For this purpose, a recently developed new molecular *ab initio* code [12] based on B splines and using the prolate spheroidal coordinate system (together with Feshbach projection) is used to evaluate the potential curves of the $Q(2)$ states for the whole R range from the molecular to the van der Waals regime. Our calculations provide a set of complete potential energy curves over the entire range of R. They also revealed that a dipole-quadrupole term, not included in earlier calculations [5,13], is significant at large distances and leads to a long range coupling of $H(2s)+H(2s)$ and $H(2s)+H(2p)$ scattering channels.

This paper is organized as follows. First, a brief description of the numerical approach for the nonperturbative calculation is given. This is followed by a discussion of perturbation theory. Then a diabatic basis for $H(n=2)+H(n'=2)$ collisions is presented. Finally, the results are given and discussed.

II. NONPERTURBATIVE APPROACH

A *B*-spline based configuration interaction (CI) method for diatomic two-electron molecules was recently implemented (see [12] for details) and is used to perform the nonperturbative calculations. In this approach the CI configurations are built with the aid of products of orbitals that are solutions of the corresponding one-electron Schrödinger equation in which the electron-electron interaction is completely neglected. The resulting one-electron problem is solved in a *B*-spline basis set in prolate spheroidal coordinates. For both the one-electron and the two-electron problem the molecular symmetry is fully taken into account. The Feshbach projection-operator approach is especially convenient for dealing with autoionizing states. In the Feshbach theory the Hilbert space is divided into two orthogonal Q and P subspaces. Their mutual interaction results in the autoionization width and an energy shift. According to [10] the energy shift is expected to be minimal, if the P subspace is constructed using the n lowest-lying solutions of the one-electron Schrödinger equation. The corresponding orthogonal Q subspace can directly be obtained by simply excluding these orbitals from the configuration space of the CI calculation. The $Q(2)$ states are obtained by omitting the two lowest lying orbitals ($1\sigma_g$ and $1\sigma_u$) from the configuration list. [This is actually the motivation for calling these states $Q(2)$ states.] Clearly, the accuracy of this procedure depends crucially on the precision of the calculated P-subspace wave functions. The present approach allows the very highly accurate evaluation of these orbitals for arbitrary internuclear distances due to the use of *B* splines and prolate spheroidal coordinates. While the one-center calculations (using *B* splines) of Martín and co-workers [11] run into numerical problems (due to slow convergence) for internuclear distances larger than 4 to $5a_0$, the traditional approaches with global atom-centered basis functions (like Gaussians) or explicitly correlated basis functions (geminals) are typically hampered by numerically caused linear dependencies that often prevent systematic basis-set-convergence investigations.

The $Q(2)$ states converge in the separated-atom limit to two hydrogen atoms with principal quantum number $n=2$, if they are adiabatically continued from small to infinite internuclear distances R. All possible combinations of H($n=2$) (with spin up and down) result in 32 singlet and triplet states. In the absence of external fields and ignoring relativistic effects there occur 22 different molecular $Q(2)$ states out of which 10 are doubly degenerate Π and Δ states. All these 22 states (converging for $R\rightarrow\infty$ to $E=-0.25$ a.u.) have been reevaluated in the present work, the calculations extending from $R=1.0a_0$ (where accurate potential curves existed before) to at least $R=100a_0$ and thus far beyond previously existing *ab initio* data. For this purpose, a careful basis-set optimization has been performed. As is discussed in [12], the efficient calculation of the potential curves requires a judicious choice of the basis-set parameters depending on the internuclear distance in order to keep the number of configurations in the CI calculation reasonably small. (Much larger CI expansions could be handled using iterative eigenvector solvers like the Davidson routine, but this is not yet implemented.)

The one-electron basis set is specified by the number n_ξ (n_η) and the order k_ξ (k_η) of the *B* splines used along the prolate spheroidal coordinates ξ (η) and the knot sequences used for the splines along those two coordinates. Each knot sequence used can be specified by a parameter g which gives the ratio between the lengths of $i+1$th and ith nonzero knot intervals. A simple uniform (linear) knot sequence corresponds to $g=1$. The maximum value of ξ, the so-called box radius $\xi_{\max}$, is an important basis-set parameter, since it determines the number (and density) of Rydberg (as well as pseudo-Rydberg) and (discretized) continuum orbitals available with a given basis. This is due to the fact that the calculation selects only those wave functions that vanish at the box boundary. Therefore, only those orbitals that decay before (bound states) or have a node (Rydberg and continuum states) at the box boundary are obtained by the calculation. The variational procedure involves $\tilde{n}_\xi=n_\xi-1$ coefficients specifying the ξ dependence of the orbitals (first coefficient is set to 0) as well as $\tilde{n}_\eta=n_\eta/2$ coefficients specifying the η dependence, the factor of 1/2 arising from the explicit requirement of the inversion symmetry. The subsequent CI calculations are performed with all or a selected number of the symmetry-adapted configurations that can be built with the $\tilde{N}=\tilde{n}_\xi\tilde{n}_\eta$ orbitals that are obtained for a given orbital symmetry ($\sigma_g,\sigma_u,\pi_g,\ldots$) in the one-electron calculation.

Since the optimal choice of basis-set parameters is R dependent, the basis-set discussion is split into three parts. First, a discussion of the basis-set optimization for short internuclear distances ($R<10a_0$) is given, followed by the consideration of very large internuclear distances ($R>70a_0$) and a brief discussion of the intermediate regime ($10a_0<R<70a_0$). For all internuclear distances convergence of the energies was monitored by a variation of all relevant basis-set parameters (like $\tilde{n}_\xi$, $\tilde{n}_\eta$, number of configurations, etc.) by at least 10%–20% of their value.

The basis-set optimization for short internuclear distances ($R<10a_0$) where electron-electron interaction (including exchange and correlation) is important follows basically the rules discussed in detail in [12]. In this regime the completeness of the selected configurations with respect to the underlying orbital basis is most important. Therefore, all possible symmetry-adapted configurations that can be formed with the aid of the obtained orbitals for a given *B*-spline basis are used, with the only restriction that the orbitals fulfill the condition $N_\eta+\lambda\leq l_{\max}$ with $l_{\max}=5$ to 6. A series of tests has shown that this choice for $l_{\max}$ leads to a convergence of the energy within at least 4 to 5 significant digits. In fact, convergence with respect to $l_{\max}$ is better for the $Q(2)$ states than for the low-lying states for which convergence was explicitly monitored in [12]. The orbital quantum numbers λ and N_η specify, respectively, the absolute value of the component of the angular momentum along the internuclear axis, $\lambda=0(\sigma),1(\pi),2(\delta),\ldots$, and the number of nodes of the η component of the orbital wave function, $N_\eta=0,\ldots,n_\eta$. In the united-atom-limit case, the atomic angular momentum l is equal to $N_\eta+\lambda$ and the condition above corresponds simply to a restriction on l. Convergence with respect to the *B*-spline parameters was obtained choosing $\tilde{n}_\eta=10$ (with a uniform knot sequence, $g=1.0$) and $\tilde{n}_\xi$ in between 10 and 15 (with a

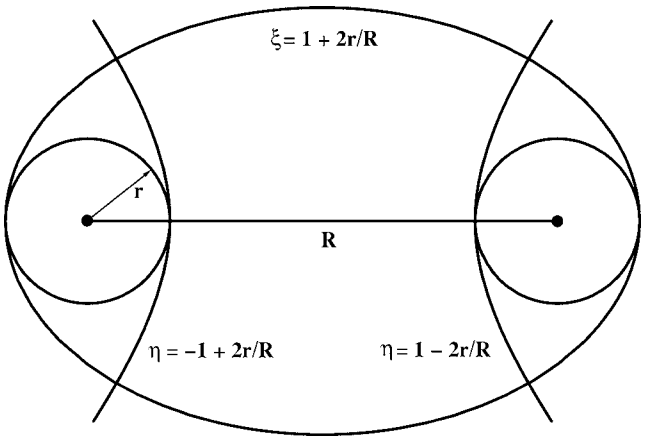

FIG. 1. Visualization of the used prolate spheroidal coordinates (ξ, η) and their relations to the distance r from the focal points.

geometrically progressive distribution, $g=1.3-1.6$). In most cases the box size $\xi_{\max}=80/R$ was chosen. However, in the range $R=1.0-3.0$ the structure and extension of the wave functions varied strongly for the different molecular states. Thus the calculations were performed for different box sizes, and the optimal box size was determined for each state separately.

The electronic density of two noninteracting $H(n=2)$ atoms is almost exclusively located within two spheres of radius $r_{n=2}=35a_0$ centered at the two nuclei. At very large internuclear separations ($R>70a_0$) the electron densities of the $Q(2)$ states of H_2 are thus very similar to the ones of two noninteracting $H(n=2)$ atoms and are only slightly distorted by the interatomic interaction. Translating this geometry into the prolate spheroidal coordinate system, the box size $\xi_{\max}=1+2r_{n=2}/R$ is chosen (see Fig. 1). Convergence with respect to ξ was achieved using $\tilde{n}_\xi=25$ and a geometrically progressive distribution characterized by $g_\xi=1.1$. For $R=70a_0$ convergence with respect to η was obtained with a uniform knot sequence and $\tilde{n}_\eta=40$. For a uniform knot sequence an increase of R leads to an increase of the length of nonzero knot intervals and, therefore, to a decrease of the number of such intervals inside $1-2r_{n=2}/R<|\eta|<1$ (see Fig. 1). Such a decrease can be compensated by an increase of $\tilde{n}_\eta$. Since the calculation of the orbitals with large $\tilde{n}_\eta$ is time-consuming, for $R>140a_0$ the value of $\tilde{n}_\eta$ was fixed at 80 and a geometrically progressive distribution was used that assures that the ratio of knot points inside the interval $|\eta|<1-2r_{n=2}/R$ does not exceed 50%. With these basis-set parameters all possible orbitals $(\tilde{N}=\tilde{n}_\xi\tilde{n}_\eta)$ for $\sigma_{g,u}, \pi_{g,u}, \delta_{g,u}$ (additionally $\phi_{g,u}$ for $R=70-100a_0$) were calculated. As for all other R values, the $1\sigma_{g,u}$ orbitals are then removed from the orbital list, if the $Q(2)$ states should be calculated. The remaining orbitals are classified according to two properties. First, they are sorted with respect to the energy value to which they converge asymptotically for $R\to\infty$. In this way the label n is introduced using the relation $E(R\to\infty)=-\frac{1}{2n^2}$. Due to the discretization (implied by the finite box size) this sorting has a physical meaning only for small n. This is, however, adequate in the present calculation of the states converging to $n=2$. The second important criterion for the configuration selection is the number of nodes N_η. Limiting N_η leads to a removal of strongly oscillating orbitals.

The configurations for the CI calculation are now constructed in the following way. One electron occupies one of the n orbitals and the other one all orbitals from the list that fulfill the symmetry requirements (correct m and inversion quantum numbers) and the condition $N_\eta\leqslant 2\kappa_n-1$ where $\{\kappa_n\}$ is an R-dependent set of natural numbers. The choice of $\{\kappa_n\}$ at some R is directly related to the choice of the configuration set used for the CI calculations at this R. In the case of the $Q(2)$ states the configurations containing two $n=2$ orbitals may be called *basic* configurations. For very large R these configurations give the main contribution to the energy but require a rather large value of κ_2 (around 20–25) to achieve convergence. Since the configurations belonging to $n=3$ add only a small correction, κ_3 is chosen around 5–10, while all $\kappa_{n>3}$ are set to 0 for $R>100a_0$. With decreasing internuclear distance R the importance of the configurations that do not belong to the basic ones grows. Therefore, κ_2 was decreased in order to allow larger κ_n for $n>2$ while retaining a reasonable size of the total number of configurations (typically, 5000–10 000 configuration for each symmetry). For $R<100a_0$ $\kappa_4\neq 0$ has to be used. Because of the different structures of the different $Q(2)$ states it is difficult to provide a general recipe for the change of $\{\kappa_n\}$ with R. Moreover, for $R=70-80a_0$ the configurations with one electron occupying an orbital with $n>4$ and the other one occupying a symmetry-allowed low-energy orbital are more important than is reflected by the selection rule based on $\{\kappa_n\}$.

As is discussed above, the intermediate regime ($10a_0<R<70a_0$) is the most difficult one, since it appears that there does not exist any simple physical picture that can serve as a guideline for optimizing the basis set. Different basis-set selection schemes were tried in this regime, but no universal one was found. The main idea for each individual state was to find a kind of an interpolation scheme between the short- and the long-range basis sets discussed above. The best results (judged on the basis of the variational principle) that were obtained with the different schemes were then used for obtaining the final potential curves.

III. PERTURBATION THEORY

For sufficiently large internuclear distances electron-electron exchange becomes negligible and the remaining electrostatic atom-atom interaction may be treated by perturbation theory. The application of perturbation theory to $H(n=2)+H(n'=2)$ collisions has been discussed previously [5,9,13]. The comparison of the present CI results with the earlier perturbative results revealed an unjustified neglect of dipole-quadrupole terms due to wrong symmetry arguments [13]. Therefore, a careful analysis of the symmetries is presented together with corrected results.

Consider a system consisting of two protons p_A, p_B with coordinates $\boldsymbol{r}_A$, $\boldsymbol{r}_B$ and two electrons e_1, e_2 with coordinates $\boldsymbol{r}_1$, $\boldsymbol{r}_2$. The internuclear coordinate is $\boldsymbol{R}=\boldsymbol{r}_B-\boldsymbol{r}_A$ and the interelectron distance $r_{12}=|\boldsymbol{r}_2-\boldsymbol{r}_1|$. The standard approach for solving the electrostatic problem starts with the introduction of atom-centered electronic coordinates. Since electrons

(protons) are indistinguishable particles, the choice of such coordinates as well as the choice of the unperturbed Hamiltonian and the perturbation is not unique. It depends on the particular arrangement channel defined by the scattering problem. For the arrangement variant $(p_A e_1)+(p_B e_2)$ the atom-centered electron coordinates are given by $\boldsymbol{\rho}_1 \equiv \boldsymbol{r}_1 - \boldsymbol{r}_A$ and $\boldsymbol{\rho}_2 \equiv \boldsymbol{r}_2 - \boldsymbol{r}_B$. The electronic Born-Oppenheimer (BO) Hamiltonian $\hat{\mathcal{H}}$ is thus divided into the unperturbed Hamiltonian

$$\hat{\mathcal{H}}_0(\boldsymbol{r}_1,\boldsymbol{r}_2) = -\frac{1}{2}\nabla^2_{\boldsymbol{\rho}_1} - \frac{1}{\rho_1} - \frac{1}{2}\nabla^2_{\boldsymbol{\rho}_2} - \frac{1}{\rho_2} \tag{1}$$

and the small perturbation

$$\hat{\mathcal{V}}(\boldsymbol{r}_1,\boldsymbol{r}_2) = -\frac{1}{|\boldsymbol{R}-\boldsymbol{\rho}_1|} - \frac{1}{|\boldsymbol{R}+\boldsymbol{\rho}_2|} + \frac{1}{R} + \frac{1}{r_{12}} = \sum_{l_1=1}^{\infty}\sum_{l_2=1}^{\infty} \frac{V_{l_1 l_2}(\boldsymbol{\rho}_1,\boldsymbol{\rho}_2)}{R^{1+l_1+l_2}}. \tag{2}$$

In Eq. (2) the quantity

$$V_{l_1 l_2}(\boldsymbol{\rho}_1,\boldsymbol{\rho}_2) = \sum_{\mu=-\min(l_1,l_2)}^{\min(l_1,l_2)} A^{\mu}_{l_1 l_2} \rho_1^{l_1} \rho_2^{l_2} Y_{l_1\mu}(\hat{\rho}_1) Y_{l_2-\mu}(\hat{\rho}_2) \tag{3}$$

with

$$A^{\mu}_{l_1 l_2} = (-1)^{l_2} 4\pi (l_1+l_2)\,!\,[(2l_1+1)(2l_2+1)]^{-1/2} \times [(l_1-\mu)\,!\,(l_1+\mu)\,!\,(l_2-\mu)\,!\,(l_2+\mu)\,!\,]^{-1/2} \tag{4}$$

has been introduced.

Since the fully molecular-symmetry adapted solutions of the perturbation problem are desired, the symmetry properties of the operators $\hat{\mathcal{H}}$, $\hat{\mathcal{H}}_0$, and $\hat{\mathcal{V}}$ have to be considered.

The electronic BO Hamiltonian $\hat{\mathcal{H}}$ is invariant under inversion $\mathcal{I}$ of all electronic coordinates with respect to the center of mass, $\boldsymbol{R}_{\rm cm}=(\boldsymbol{r}_A+\boldsymbol{r}_B)/2$, to electron exchange $\mathcal{P}_{12}$, and to a reflection $\mathcal{R}$ by a plane containing the protons.

The transformation $\mathcal{R}$ does not change r_{12} and the length of vectors $\boldsymbol{\rho}_i$ and $\boldsymbol{R}\pm\boldsymbol{\rho}_i$, where $i=1,2$. It follows from Eqs. (1) and (2) that both $\hat{\mathcal{H}}_0$ and $\hat{\mathcal{V}}$ are invariant with respect to $\mathcal{R}$.

The action of the transformations $\mathcal{I}$ and $\mathcal{P}_{12}$ on the coordinates is given by

$$\begin{aligned} \mathcal{I}\text{:}\quad & \boldsymbol{r}_1 \to 2\boldsymbol{R}_{\rm cm} - \boldsymbol{r}_1 \Leftrightarrow \boldsymbol{\rho}_1 \to \boldsymbol{R} - \boldsymbol{\rho}_1 \\ & \boldsymbol{r}_2 \to 2\boldsymbol{R}_{\rm cm} - \boldsymbol{r}_2 \Leftrightarrow \boldsymbol{\rho}_2 \to -\boldsymbol{R} - \boldsymbol{\rho}_2 \\ \mathcal{P}_{12}\text{:}\quad & \boldsymbol{r}_1 \to \boldsymbol{r}_2 \Leftrightarrow \boldsymbol{\rho}_1 \to \boldsymbol{\rho}_2 + \boldsymbol{R} \\ & \boldsymbol{r}_2 \to \boldsymbol{r}_1 \Leftrightarrow \boldsymbol{\rho}_2 \to \boldsymbol{\rho}_1 - \boldsymbol{R} \end{aligned} \tag{5}$$

Neither $\hat{\mathcal{H}}_0$ nor $\hat{\mathcal{V}}$ is invariant with respect to the transformations $\mathcal{I}$ and $\mathcal{P}_{12}$. This means that the full set of molecular quantum numbers cannot be used to specify the unperturbed solutions. A maximal use of symmetry is possible by the construction of the symmetry transformation both for $\hat{\mathcal{H}}_0$ and $\hat{\mathcal{V}}$ as well as $\hat{\mathcal{H}}$. The easiest choice is the transformation $\mathcal{B}$ defined as

$$\mathcal{B} = \mathcal{P}_{12}\mathcal{I} = \mathcal{I}\mathcal{P}_{12}. \tag{6}$$

Indeed, the action of $\mathcal{B}$ on the coordinates is given by

$$\begin{aligned} \mathcal{B}\text{:}\quad & \boldsymbol{r}_1 \to 2\boldsymbol{R}_{\rm cm} - \boldsymbol{r}_2 \Leftrightarrow \boldsymbol{\rho}_1 \to -\boldsymbol{\rho}_2 \\ & \boldsymbol{r}_1 \to 2\boldsymbol{R}_{\rm cm} - \boldsymbol{r}_1 \Leftrightarrow \boldsymbol{\rho}_2 \to -\boldsymbol{\rho}_1 \end{aligned} \tag{7}$$

and it follows from Eqs. (1) and (2) that both $\hat{\mathcal{H}}_0$ and $\hat{\mathcal{V}}$ are invariant with respect to $\mathcal{B}$.

The full set of H_2 quantum numbers is given by $\boldsymbol{\tau} \equiv \{M, p_i, p_s, [p_r]\}$, where M is the orbital angular-momentum projection quantum number and p_i, p_s, and p_r are the parities with respect to $\mathcal{I}$, $\mathcal{P}_{12}$, and $\mathcal{R}$, respectively. The reduced set of quantum numbers used to describe eigenvectors of $\hat{\mathcal{H}}_0$ and $\hat{\mathcal{H}}$ is then $\tau \equiv \{M, p_\beta, [p_r]\}$, where the parity p_β is connected with p_i, p_s by the relation

$$p_\beta = p_i p_s. \tag{8}$$

It is equal to 1 (−1) for ${}^1X_g, {}^3X_u$ (${}^1X_u, {}^3X_g$) states where X stands for $\Sigma^+, \Sigma^-, \Pi, \Delta, \ldots$. The new state symbol $X_\pm$ is used in the following to specify τ, where the subscript of $X_\pm$ denotes the parity $p_\beta = \pm 1$. Using Eq. (8) the set $\boldsymbol{\tau}$ can be also specified as $\boldsymbol{\tau} = \{p_s, \tau\}$.

The orthonormal set $\{|\{i\}\tau\rangle\}$ of symmetry-adapted eigenvectors of the unperturbed Hamiltonian $\hat{\mathcal{H}}_0$ (with the eigenvalue $E^{(0)} = -0.25$ a.u.) is given by

$$|\{1\}\Sigma^+_+\rangle = |2s\ 2s\rangle, \tag{9}$$

$$|\{2\}\Sigma^+_+\rangle = |2p^0\ 2p^0\rangle, \tag{10}$$

$$|\{3\}\Sigma^+_+\rangle = \frac{1}{\sqrt{2}}(|2s\ 2p^0\rangle - |2p^0\ 2s\rangle), \tag{11}$$

$$|\{4\}\Sigma^+_+\rangle = \frac{1}{\sqrt{2}}(|2p^-2p^+\rangle + |2p^+2p^-\rangle), \tag{12}$$

$$|\{1\}\Sigma^+_-\rangle = \frac{1}{\sqrt{2}}(|2s\ 2p^0\rangle + |2p^0\ 2s\rangle), \tag{13}$$

$$|\{1\}\Sigma^-_-\rangle = \frac{1}{\sqrt{2}}(|2p^-2p^+\rangle - |2p^+2p^-\rangle), \tag{14}$$

$$|\{1\}\Pi_+\rangle = \frac{1}{\sqrt{2}}(|2s\ 2p^+\rangle - |2p^+2s\rangle), \tag{15}$$

$$|\{2\}\Pi_+\rangle = \frac{1}{\sqrt{2}}(|2p^0\ 2p^+\rangle + |2p^+2p^0\rangle), \tag{16}$$

$$|\{1\}\Pi_-\rangle = \frac{1}{\sqrt{2}}(|2p^0\ 2p^+\rangle - |2p^+2p^0\rangle), \tag{17}$$

$$|\{2\}\Pi_-\rangle = \frac{1}{\sqrt{2}}(|2s\ 2p^+\rangle + |2p^+2s\rangle), \tag{18}$$

$$|\{1\}\Delta_+\rangle = |2p^+2p^+\rangle, \tag{19}$$

where the index $i=1,\ldots,g_\tau$ enumerates a basis state with symmetry τ and g_τ specifies the dimension of the degenerate subspace with symmetry τ. Due to symmetry only states with the same value of τ are coupled by the perturbation $\hat{\mathcal{V}}$. The calculation of the matrices $V_{ji}(\tau) \equiv \langle\{j\}\tau|\hat{\mathcal{V}}|\{i\}\tau\rangle$ yields

$$V(\Sigma_+^+) = \begin{pmatrix} 0 & -\frac{18}{R^3} & 0 & -\frac{9\sqrt{2}}{R^3} \\ -\frac{18}{R^3} & \frac{864}{R^5} & -\frac{108\sqrt{2}}{R^4} & \frac{432\sqrt{2}}{R^5} \\ 0 & -\frac{108\sqrt{2}}{R^4} & \frac{18}{R^3} & -\frac{108}{R^4} \\ -\frac{9\sqrt{2}}{R^3} & \frac{432\sqrt{2}}{R^5} & -\frac{108}{R^4} & \frac{432}{R^5} \end{pmatrix},$$

$$V(\Sigma_-^+) = \left(-\frac{18}{R^3}\right); \quad V(\Sigma_-^-) = (0); \quad V(\Delta_+) = \left(\frac{216}{R^5}\right),$$

$$V(\Pi_+) = \begin{pmatrix} -\frac{9}{R^3} & \frac{108}{R^4} \\ \frac{108}{R^4} & -\frac{864}{R^5} \end{pmatrix}; \quad V(\Pi_-) = \begin{pmatrix} 0 & 0 \\ 0 & \frac{9}{R^3} \end{pmatrix}. \tag{20}$$

In the previous implementation of perturbation theory in [13], the dipole-quadrupole interaction (being proportional to R^{-4}) was postulated to vanish for symmetry reasons. In [13] an "inner parity" P_0 is introduced that corresponds in the present notations to the transformation $\boldsymbol{\rho}_i \to -\boldsymbol{\rho}_i$, $i=1,2$. Since the dipole-dipole term is invariant with respect to this transformation, the parity P_0 was used to classify the different states. It was correctly concluded that "the dipole-quadrupole interaction anticommutes with the operator P_0 as a result of which all its diagonal matrix elements computed with functions of definite P_0 parity vanish" [13]. However, it was overlooked that the anticommutation property allows for a coupling of states with opposite P_0 parity (but same τ). Also in [9] the terms in Eq. (20) that are proportional to R^{-4} were neglected and, therefore, transitions between $H(2s)+H(2p)$ and $H(2p)+H(2p)$ were forbidden. The new perturbative results show, however, that the $H(2s)+H(2p)$ collisional channel should be taken into account in scattering calculations involving channels that couple either directly or indirectly to the $H(2s)+H(2p)$ channel, as is, e.g., the case for $H(2s)+H(2s)$ collisions.

In the nondegenerate case ($g_\tau=1$) the first-order energy correction is given by $E_1^{(1)}(R;\tau)=V_{11}(\tau)$. For $g_\tau>1$ the zeroth-order wavefunctions $|\alpha\tau\rangle^{(0)}$ are given by

$$|\alpha\tau\rangle^{(0)} = \sum_{i=1}^{g_\tau} U_{i\alpha}^{(0)}(R;\tau)|\{i\}\tau\rangle \quad \text{for } \alpha = 1,\ldots,g_\tau \tag{21}$$

where $U_{i\alpha}^{(0)}(R;\tau)$ together with the first-order energy corrections $E_\alpha^{(1)}(R;\tau)$ are obtained from a diagonalization of $V(\tau)$.

TABLE I. Perturbation theory: Calculated van der Waals coefficients $C_{\alpha;n}^{(k)}(\tau)$ of the $Q(2)$ states for all symmetries τ. Here α, k, and n specify the state index, the order of the perturbation theory, and the inverse power of R with which $C_{\alpha;n}^{(k)}(\tau)$ is multiplied, respectively.

τ[a]	α	$C_3=C_{\alpha,3}^{(1)}$	$C_5=C_{\alpha,5}^{(1)}$	$C_{\alpha,7}^{(1)}$	$C_6=C_{\alpha,6}^{(2)}$
Σ_+^+	1	$-9\sqrt{6}$	$324(8-3\sqrt{6})$	$1944(-1224+499\sqrt{6})$	−6737
	2	0	0	0	−6718
	3	18	−3888	4758912	−8783
	4	$9\sqrt{6}$	$324(8+3\sqrt{6})$	$1944(-1224-499\sqrt{6})$	−6737
Σ_-^+	1	−18	0	0	−8783
Σ_-^-	1	0	0	0	−1824
Π_+	1	−9	−1296	62208	−6165
	2	0	432	−62208	−3062
Π_-	1	0	0	0	−7501
	2	9	0	0	−6165
Δ_+	1	0	216	0	−4042

[a]The reduced set of quantum numbers τ is related to the full set of H_2 quantum numbers as: $\Sigma_+^+ \to {}^1\Sigma_g^+, {}^3\Sigma_u^+$, $\Sigma_-^+ \to {}^1\Sigma_u^+, {}^3\Sigma_g^+$, etc.

Note, the energies $E_\alpha^{(1)}(R;\tau)$ obtained this way are odd functions of R despite the occurrence of the R^{-4} terms in the interaction matrices V in Eq. (20). An example is

$$E_1^{(1)}(R;\Pi_+) = -\frac{432}{R^5} - \frac{9}{2R^3}\left(1+\sqrt{1+\frac{384}{R^2}+\frac{9216}{R^4}}\right). \tag{22}$$

Therefore, it is possible to make an expansion of $E_\alpha^{(1)}(R;\tau)$ containing only odd powers of R,

$$E_\alpha^{(1)}(R;\tau) = \frac{C_{\alpha;3}^{(1)}(\tau)}{R^3} + \frac{C_{\alpha;5}^{(1)}(\tau)}{R^5} + \frac{C_{\alpha;7}^{(1)}(\tau)}{R^7} + \cdots \tag{23}$$

with the van der Waals coefficients $C_{\alpha;n}^{(1)}(\tau)$ that are listed in Table I.

The degeneracy is now completely removed for every τ and no higher-order matrix elements have to be considered for a proper construction of zeroth-order wave functions.

The functions $U_{i\alpha}^{(0)}(R;\tau)$ can be analyzed by expanding them in a power series of R^{-1}

$$U_{i\alpha}^{(0)}(R;\tau) = U_{i\alpha;0}^{(0)}(\tau) + U_{i\alpha;1}^{(0)}(\tau)R^{-1} + U_{i\alpha;2}^{(0)}(\tau)R^{-2} + \cdots. \tag{24}$$

The expansion coefficients $U_{i\alpha;j}^{(0)}(\tau)$ for $j=0,1,2$ are presented in Table II.

Table I shows that some of the states have vanishing first-order corrections, i.e., all first-order van der Waals coefficients are zero. In order to reveal the first nonvanishing contribution the second-order correction has to be calculated. Because of the metastable character of resonant states the application of second-order perturbation theory requires the use of a partitioning technique. The formalism and numerical

TABLE II. Perturbation theory: Coefficients of the expansion (24) for the quantum numbers τ with $g_\tau > 1$.

τ	α	i	$U^{(0)}_{i\alpha;0}$	$U^{(0)}_{i\alpha;1}$	$U^{(0)}_{i\alpha;2}$
Σ^+_+	1	1	$\sqrt{1/2}$	0	$-(162\sqrt{2}-132\sqrt{3})$
		2	$\sqrt{1/3}$	0	$-\sqrt{2}(36\sqrt{6}-84)$
		3	0	$18-6\sqrt{6}$	0
		4	$\sqrt{1/6}$	0	$-(36\sqrt{6}-84)$
	2	1	0	0	0
		2	$-\sqrt{1/3}$	0	0
		3	0	0	0
		4	$\sqrt{2/3}$	0	0
	3	1	0	$-18\sqrt{2}$	0
		2	0	$12\sqrt{2}$	0
		3	1	0	−540
		4	0	12	0
	4	1	$\sqrt{1/2}$	0	$-(162\sqrt{2}+132\sqrt{3})$
		2	$-\sqrt{1/3}$	0	$\sqrt{2}(36\sqrt{6}+84)$
		3	0	$18+6\sqrt{6}$	0
		4	$-\sqrt{1/6}$	0	$36\sqrt{6}+84$
Π_+	1	1	1	0	−72
		2	0	−12	0
	2	1	0	12	0
		2	1	0	−72
Π_-	1	1	1	0	0
		2	0	0	0
	2	1	0	0	0
		2	1	0	0

analysis of such a problem will be discussed in detail elsewhere. In this work only the leading second-order van der Waals coefficients $C^{(2)}_{\alpha;6}(\tau)$ are reported (Table I) to allow a comparison of the nonperturbative and perturbative results. Note, for the $|1\Sigma^+_+\rangle$ state the R^{-6} term dominates over the R^{-5} term for $R < 32a_0$. Therefore, even in the case of nonvanishing first-order corrections the second-order correction can be important.

IV. DIABATIC BASIS

If atomic collisions are considered in the framework of coupled-channel theory, some R-dependent electronic basis set is required. The adiabatic basis set has been discussed in Sec. II. However, standard formulations of coupled-channel theory are based on diabatic basis sets. The aim of this section is to discuss a possible diabatic basis and its relation to the adiabatic one. This is important, if the nonperturbative potential curves are to be used for scattering calculations.

For $H(n=2)+H(n'=2)$ collisions a tempting choice for a diabatic basis is given by Eqs. (9)–(19). Such a basis is implicitly R dependent, since it consists of atomic orbitals centered at the moving nuclei. However, this basis is not sufficient to describe the electron exchange reactions. A basis that does so can be obtained by adding the set $\{\hat{\mathcal{P}}_{12}|\{i\}\tau\rangle\}$ of symmetry-adapted eigenvectors of the Hamiltonian $\hat{\mathcal{P}}_{12}\hat{\mathcal{H}}_0\hat{\mathcal{P}}_{12}$ which is the free Hamiltonian describing the arrangement $(p_A e_2)+(p_B e_1)$. From this the orthonormal set $\{|\{i\}\boldsymbol{\tau}\rangle\}$ of functions adapted to the molecular symmetry,

$$|\{i\}\boldsymbol{\tau}\rangle = \frac{1}{\sqrt{2}}[\hat{1} + p_s\hat{\mathcal{P}}_{12}]\sum_{j=1}^{g_\tau} A_{ij}(R;\boldsymbol{\tau})|\{j\}\tau\rangle, \tag{25}$$

can be constructed as the diabatic basis. The coefficients $A_{ij}(R;\boldsymbol{\tau})$ are functions of the exchange matrix elements $\langle\{i\}\tau|\hat{\mathcal{P}}_{12}|\{j\}\tau\rangle$ and for large R satisfy the condition $A_{ij}(R;\boldsymbol{\tau}) \to \delta_{ij}$ (see Appendix for details).

The diabatic basis is still incomplete, since it contains only atomic states with $n=2$. This introduces a further complication, if the results obtained with the diabatic basis are compared to the ones yielded in a fully converged adiabatic calculation as presented in Sec. II. In turn, the adiabatic wave functions $|\alpha\boldsymbol{\tau}\rangle$ can be used to estimate the degree of completeness of the diabatic basis $\{|\{i\}\boldsymbol{\tau}\rangle\}$. For this purpose one can introduce a measure of completeness

$$\Omega_\alpha(R;\boldsymbol{\tau}) = 1 - \sum_{i=1}^{g_\tau} |U_{i\alpha}(R;\boldsymbol{\tau})|^2 \tag{26}$$

with the projection coefficients $U_{i\alpha}(R;\boldsymbol{\tau}) = \langle\{i\}\boldsymbol{\tau}|\alpha\boldsymbol{\tau}\rangle$.

It can be shown that for large R the projection coefficients satisfy

$$U_{i\alpha}(R;\boldsymbol{\tau}) \to U^{(0)}_{i\alpha}(R;\tau), \tag{27}$$

if an appropriate phase convention is used for $|\alpha\boldsymbol{\tau}\rangle$. Equation (27) allows a direct comparison of the perturbatively and nonperturbatively calculated wave functions.

V. RESULTS

For small R (especially $R \leqslant 4a_0$) a number of previous calculations of the $Q(2)$ states exist [5,8–11]. Table III compares the present results with those data at some selected values of R in between 3 and $6a_0$.

In Fig. 2 all 22 $Q(2)$ potential curves of H_2 with $M \geqslant 0$ are also shown graphically for $3a_0 \leqslant R \leqslant 16a_0$. In contrast to the electronic ground state of H_2 and H_2^+ the potential minima, where they exist, are located in this range of R values. Therefore, in the case of the $Q(2)$ states it is this range of R values that deserves the name molecular regime. Transitions from the electronic ground state of H_2 usually end up in the dominantly repulsive short-range part of the $Q(2)$ states due to the Franck-Condon factors, but there exist reports on the experimental detection (and population) of long-range states of H_2 [14]. On the other hand, scattering processes like collisions of two excited hydrogen atoms are also sensitive to this molecular regime in which the potential curves can be either repulsive or attractive. For this reason the potential curves of the $Q(2)$ states had been calculated for $R > 4a_0$ before [9]. For the states with $^1\Sigma^+_g$ symmetry Fig. 2(a) shows a comparison of the present data to the results obtained with the complex-scaling method using geminals [9] and with a Feshbach projection technique using a Gaussian CI calcula-

TABLE III. Energies of the $Q(2)$ states for short internuclear distances R.

State	$R=3.0a_0$	$R=4.0a_0$	$R=5.0a_0$	$R=6.0a_0$	State	$R=3.0a_0$	$R=4.0a_0$	$R=5.0a_0$	$R=6.0a_0$
$1\,^1\Sigma_g^+$	−0.211 67[a]	−0.249 69[a]	−0.266 79[a]	−0.279 29[a]	$1\,^3\Sigma_u^+$	−0.134 04[a]	−0.189 40[a]	−0.218 96[a]	−0.243 71[a]
	−0.206 94[b]	−0.245 95[b]	−0.263 50[b]	−0.274 91[b]		−0.132 01[b]	−0.187 17[b]	−0.215 84[b]	−0.236 00[b]
	−0.209 36[c]	−0.248 06[c]	−0.266 28[c]	−0.279 92[c]		−0.126 53[e]	−0.181 32[e]	−0.218 21[c]	−0.242 03[c]
	−0.199 19[d]	−0.249 33[d]	−0.265 73[d]	−0.278 51[d]		−0.121 76[f]	−0.178 18[f]		−0.231 30[e]
	−0.188 56[f]	−0.236 38[e]		−0.265 76[e]					
		−0.226 98[f]							
$2\,^1\Sigma_g^+$	−0.138 88[a]	−0.186 86[a]	−0.215 08[a]	−0.243 38[a]	$2\,^3\Sigma_u^+$	−0.110 86[a]	−0.171 10[a]	−0.207 02[a]	−0.228 60[a]
	−0.136 18[b]	−0.184 69[b]	−0.212 50[b]	−0.235 79[b]		−0.107 88[b]	−0.167 62[b]	−0.201 93[b]	−0.225 02[b]
	−0.138 28[c]	−0.186 49[c]	−0.214 96[c]	−0.241 50[c]		−0.089 71[f]	−0.139 23[f]	−0.205 45[c]	−0.227 90[c]
	−0.105 16[f]	−0.186 15[d]	−0.214 39[d]	−0.242 22[d]					
		−0.151 58[f]							
$3\,^1\Sigma_g^+$	−0.109 58[a]	−0.157 15[a]	−0.206 79[a]	−0.235 36[a]	$3\,^3\Sigma_u^+$	−0.090 39[a]	−0.140 35[a]	−0.189 71[a]	−0.213 29[a]
	−0.10816[b]	−0.154 65[b]	−0.200 82[b]	−0.231 50[b]		−0.089 71[b]	−0.139 60[b]	−0.183 43[b]	−0.207 70[b]
	−0.108 88[c]	−0.155 77[c]	−0.205 80[c]	−0.235 17[c]				−0.189 23[c]	−0.213 23[c]
		−0.155 73[d]	−0.205 82[d]	−0.234 15[d]					
$4\,^1\Sigma_g^+$	−0.087 74[a]	−0.153 86[a]	−0.195 87[a]	−0.216 54[a]	$4\,^3\Sigma_u^+$	−0.076 03[a]	−0.133 66[a]	−0.162 58[a]	−0.189 27[a]
	−0.087 07[b]	−0.151 63[b]	−0.190 47[b]	−0.211 13[b]		−0.075 74[b]	−0.127 80[b]	−0.161 72[b]	−0.183 31[b]
	−0.085 71[c]	−0.155 40[c]	−0.195 75[c]	−0.216 27[c]				−0.161 20[c]	−0.188 71[c]
		−0.155 36[d]	−0.194 76[d]	−0.215 79[d]					
$1\,^1\Sigma_u^+$	−0.117 16[a]	−0.168 95[a]	−0.205 09[a]	−0.238 85[a]	$1\,^3\Sigma_g^+$	−0.121 11[a]	−0.170 96[a]	−0.220 94[a]	−0.251 35[a]
	−0.115 70[b]	−0.166 74[b]	−0.199 97[b]	−0.231 22[b]		−0.120 57[b]	−0.168 19[b]	−0.214 67[b]	−0.243 77[b]
	−0.106 07[e]	−0.156 20[e]		−0.210 34[e]		−0.110 24[e]	−0.150 89[e]		−0.198 86[e]
	−0.105 01[f]	−0.151 53[f]				−0.116 71[f]	−0.161 18[f]		
$1\,^1\Pi_g^+$	−0.155 15[a]	−0.205 85[a]	−0.228 63[a]	−0.239 83[a]	$1\,^3\Pi_u^+$	−0.205 40[a]	−0.240 84[a]	−0.258 85[a]	−0.276 63[a]
	−0.153 47[b]	−0.203 85[b]	−0.226 12[b]	−0.236 45[b]		−0.202 25[b]	−0.237 39[b]	−0.253 23[b]	−0.269 58[b]
	−0.145 40[e]	−0.204 85[d]	−0.227 73[d]	−0.239 07[d]		−0.194 85[e]	−0.229 38[e]		−0.260 24[e]
	−0.149 21[f]	−0.193 80[e]		−0.230 95[e]		−0.198 71[f]	−0.232 88[f]		
		−0.197 23[f]							
$2\,^1\Pi_g^+$	−0.100 30[a]	−0.148 75[a]	−0.181 84[a]	−0.220 21[a]	$2\,^3\Pi_u^+$	−0.133 97[a]	−0.202 39[a]	−0.239 94[a]	−0.249 44[a]
	−0.099 69[b]	−0.147 97[b]	−0.176 02[b]	−0.213 78[b]		−0.131 71[b]	−0.199 04[b]	−0.237 66[b]	−0.247 72[b]
	−0.098 01[f]	−0.148 14[d]	−0.181 00[d]	−0.219 50[d]		−0.126 76[f]	−0.194 08[f]		
		−0.145 08[f]							
$1\,^1\Pi_u^+$	−0.180 51[a]	−0.220 99[a]	−0.238 96[a]	−0.253 27[a]	$1\,^3\Pi_g^+$	−0.152 99[a]	−0.203 64[a]	−0.226 83[a]	−0.239 36[a]
	−0.178 17[b]	−0.218 84[b]	−0.236 29[b]	−0.249 04[b]		−0.150 07[b]	−0.200 52[b]	−0.223 44[b]	−0.235 26[b]
	−0.157 45[e]	−0.220 19[d]	−0.237 96[d]	−0.251 82[d]		−0.142 36[e]	−0.202 47[d]	−0.225 62[d]	−0.238 21[d]
	−0.166 41[f]	−0.195 08[e]		−0.223 08[e]		−0.147 21[f]	−0.189 72[e]		−0.222 21[e]
		−0.207 58[f]					−0.196 08[f]		
$2\,^1\Pi_u^+$	−0.127 39[a]	−0.187 40[a]	−0.222 78[a]	−0.237 82[a]	$2\,^3\Pi_g^+$	−0.099 21[a]	−0.147 76[a]	−0.177 18[a]	−0.214 06[a]
	−0.124 97[b]	−0.184 56[b]	−0.219 22[b]	−0.234 42[b]		−0.098 39[b]	−0.146 88[b]	−0.169 84[b]	−0.204 30[b]
	−0.115 61[f]	−0.185 69[d]	−0.220 99[d]	−0.236 44[d]		−0.097 26[f]	−0.147 16[d]	−0.176 39[d]	−0.213 65[d]
		−0.167 88[f]					−0.144 63[f]		
$1\,^1\Delta_g^+$	−0.214 53[a]	−0.251 06[a]	−0.263 06[a]	−0.265 53[a]	$1\,^3\Delta_u^+$	−0.129 66[a]	−0.185 95[a]	−0.214 68[a]	−0.230 54[a]
	−0.210 60[b]	−0.247 68[b]	−0.260 44[b]	−0.263 32[b]		−0.128 51[b]	−0.184 70[b]	−0.213 49[b]	−0.229 36[b]
	−0.197 86[f]	−0.235 58[f]				−0.114 51[f]	−0.160 53[f]		

[a]Present calculation.
[b]Feshbach theory using one-center B-spline basis functions [11].
[c]Complex-scaling method with explicitly correlated basis functions (geminals) [9].
[d]Feshbach theory using an in comparison to [10] extended two-centered Gaussian basis set [5].
[e]Feshbach theory using two-centered Gaussian basis functions [10].
[f]R-matrix theory [8].

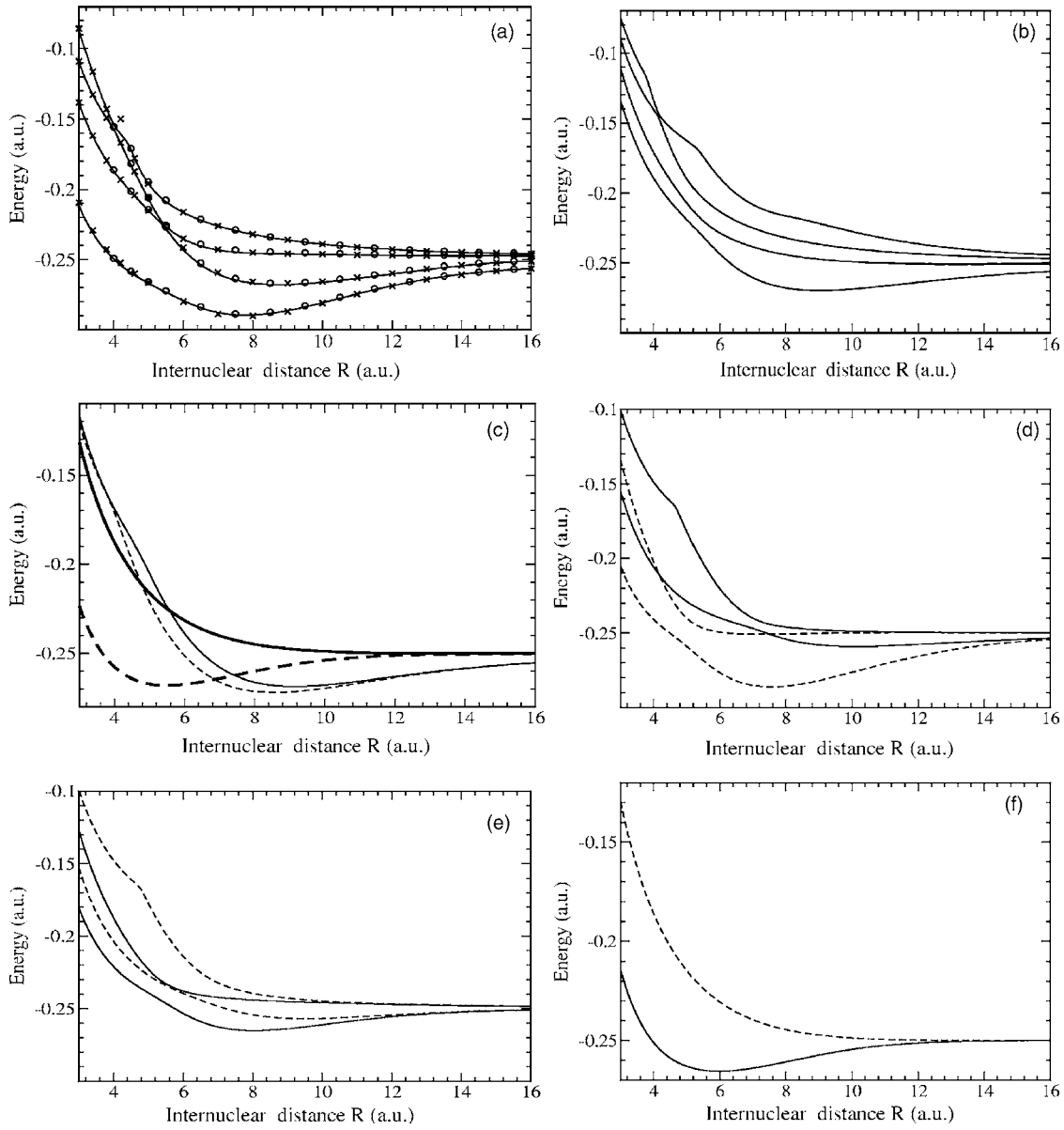

FIG. 2. The 22 $Q(2)$ potential curves (with $M \geqslant 0$) of H_2: (a) Potential energy curves of the $Q(2)$ states of H_2 with $^1\Sigma_g^+$ symmetry. Shown is a comparison of three different calculations: Present B-spline calculation using Feshbach theory (solid), a calculation using Cartesian Gaussians and Feshbach theory [5] (crosses), and a complex-scaling calculation [9] using explicitly correlated basis functions (circles). (b) Energy of $^1\Sigma_u^+$ states. (c) Energy of states for different symmetries (solid thick: $^1\Sigma_u^+$, dash thick: $^3\Sigma_g^+$, solid thin: $^1\Sigma_u^-$, dash thick: $^3\Sigma_g^-$). (d) Energy of $^1\Pi_g$ (solid) and $^3\Pi_u$ (dash) states. (e) Energy of $^1\Pi_u$ (solid) and $^3\Pi_g$ (dash) states. (f) Energy of $^1\Delta_g$ (solid) and $^3\Delta_u$ (dash) states.

tion. (This calculation was used for obtaining the non-Σ states and in the scattering calculation in [5].) The overall agreement of the present results with the ones obtained using the complex-scaling method visible from Table III and Fig. 2(a) for larger internuclear distances ($R > 4.0a_0$) is a clear indication of the decreasing size of the energy shift (arising from the interaction between Q and P subspaces), since this shift is automatically present in the complex-scaling calculation. From the numerical values given in Table III it is also apparent that the present results are for larger internuclear distances in better overall agreement with the geminal complex-scaling calculation in [9] than with the one-center Feshbach approach used in [11]. This is in accordance with the expectation of slow convergence of one-center approaches for large internulear distances. According to Fig. 2(a) the present results also agree very well with the previous Gaussian CI calculation [5]. However, a careful analysis reveals problems in the latter calculation, especially for large internuclear distances. This is demonstrated in Fig. 3 where (on a much more enlarged scale) the present results for some states of $^1\Pi_u$ symmetry are compared to the previous Gaussian results [5]. (No geminal data exist for states with non-Σ symmetry.) While the present results asymptotically converge to their correct limit (−0.25 a.u.), this is not the case for the Gaussian ones. Although the shape of the potential curves obtained with the Gaussians is very similar to the present ones, they have different energy off-sets, as is clearly visible from the different asymptotes. More seriously, this

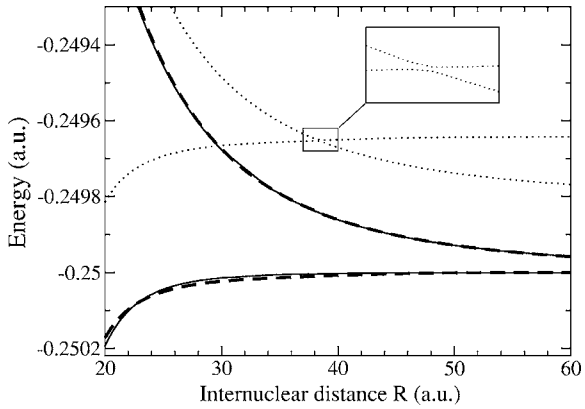

FIG. 3. Energy of $^1\Pi_u$ states when calculated with different numerical approaches: Present B-spline calculation (solid), and a previous Gaussian calculation [5] (points: Raw data, dashed: The same but energy shifted).

energy off-set differs for different states of the same symmetry (and obtained with the same basis set). As a result, the Gaussian results show an unphysical avoided crossing. The fatal consequences of such an unphysical behavior for low-energy scattering calculations should be evident. Although in the calculations in [5] the existence of this off-set and the absence of the avoided crossing were recognized and allowed for, the more accurate calculations provided by the present results are needed for reliable predictions of the scattering process.

The potential curves of the $Q(2)$ states for large internuclear distances are presented in Fig. 4. In order to emphasize the asymptotic long-range behavior the potential curves are plotted as a function of $(E+0.25)R^3$ versus the inverse internuclear distance R^{-1}. Plotted this way the energy curves should converge for $R^{-1}\rightarrow 0$ to the value of the corresponding C_3 van der Waals coefficient. As can be seen from Fig. 4,

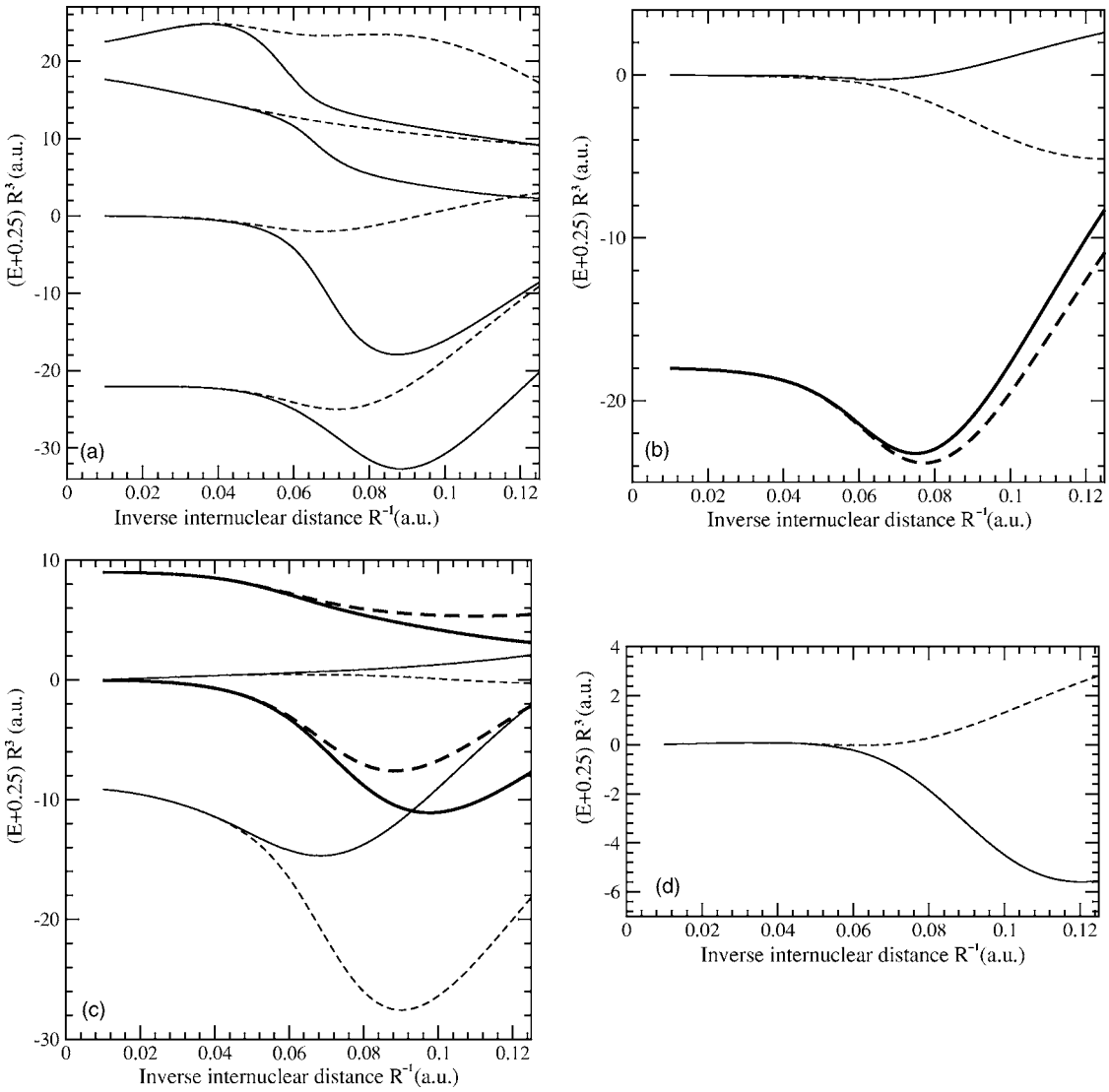

FIG. 4. Energies of the $Q(2)$ states of H_2 obtained with the nonperturbative CI calculation. In order to connect the results with the long-range behavior predicted by the perturbation theory the energies are plotted vs the inverse internuclear distance R, shifted by 0.25 a.u., and multiplied by R^3. Plotted this way, the curves converge to the van der Waals C_3 coefficients for $R^{-1}\rightarrow 0$ (see Table I). (a) $^1\Sigma_g^+$ (solid) and $^3\Sigma_u^+$ (dash) symmetry. (b) $^1\Sigma_u^+$ (thick solid curve), $^3\Sigma_g^+$ (thick dashes), $^1\Sigma_u^-$ (thin solid), and $^3\Sigma_g^-$ (thin dashes). (c) $^1\Pi_u$ (thick solid curve), $^3\Pi_g^+$ (thick dashes), $^1\Pi_g$ (thin solid), and $^3\Sigma_u$ (thin dashes). (d) $^1\Delta_g$ (solid) and $^3\Delta_u$ (dash).

TABLE IV. Energies of the $Q(2)$ states for large internuclear distances R.

R (units of a_0)	$1\,^1\Sigma_g^+$	$2\,^1\Sigma_g^+$	$3\,^1\Sigma_g^+$	$4\,^1\Sigma_g^+$	$1\,^1\Sigma_u^+$
80.0	−0.250 043 043 908[a]	−0.250 000 050 608[a]	−0.249 965 917 821[a]	−0.249 955 663 782[a]	−0.250 035 225 919[a]
	−0.250 043 018 873[b]	−0.250 000 025 627[b]	−0.249 965 891 914[b]	−0.249 955 622 359[b]	−0.250 035 189 754[b]
90.0	−0.250 030 233 004[a]	−0.250 000 028 049[a]	−0.249 975 922 156[a]	−0.249 969 031 692[a]	−0.250 024 730 725[a]
	−0.250 030 217 611[b]	−0.250 000 012 641[b]	−0.249 975 904 390[b]	−0.249 969 009 043[b]	−0.250 024 707 885[b]
100.0	−0.250 022 041 050[a]	−0.250 000 016 746[a]	−0.249 982 370 561[a]	−0.249 977 516 867[a]	−0.250 018 021 780[a]
	−0.250 022 031 068[b]	−0.250 000 006 718[b]	−0.249 982 358 228[b]	−0.249 977 503 361[b]	−0.250 018 008 783[b]
150.0	−0.250 006 531 530[a]	−0.250 000 002 472[a]	−0.249 994 718 647[a]	−0.249 993 407 618[a]	−0.250 005 336 800[a]
	−0.250 006 529 786[b]	−0.250 000 000 590[b]	−0.249 994 716 095[b]	−0.249 993 405 673[b]	−0.250 005 334 104[b]
200.0	−0.250 002 755 502[a]	−0.250 000 000 615[a]	−0.249 997 762 598[a]	−0.249 997 229 626[a]	−0.250 002 250 814[a]
	−0.250 002 755 122[b]	−0.250 000 000 105[b]	−0.249 997 761 935[b]	−0.249 997 229 241[b]	−0.250 002 250 137[b]
R (units of a_0)	$1\,^1\Pi_g^+$	$2\,^1\Pi_g^+$	$1\,^1\Pi_u^+$	$2\,^1\Pi_u^+$	$1\,^1\Delta_g^+$
88.0	−0.250 013 463 614[a]	−0.249 999 949 925[a]	−0.250 000 040 912[a]	−0.249 986 806 031[a]	−0.249 999 967 668[a]
	−0.250 013 464 074[b]	−0.249 999 926 219[b]	−0.250 000 016 152[b]	−0.249 986 806 570[b]	−0.249 999 967 774[b]
96.0	−0.250 010 337 535[a]	−0.249 999 968 227[a]	−0.250 000 026 572[a]	−0.249 989 834 374[a]	−0.249 999 978 493[a]
	−0.250 010 338 537[b]	−0.249 999 951 741[b]	−0.250 000 009 583[b]	−0.249 989 835 350[b]	−0.249 999 978 673[b]
100.0	−0.250 009 133 834[a]	−0.249 999 974 242[a]	−0.250 000 021 583[a]	−0.249 991 004 931[a]	−0.249 999 982 224[a]
	−0.250 009 135 155[b]	−0.249 999 960 472[b]	−0.250 000 007 501[b]	−0.249 991 006 165[b]	−0.249 999 982 442[b]

[a]Present calculation.

[b]Prediction of the perturbation theory (first-order term plus the leading second-order term that varies as R^{-6}).

the CI results are in very good agreement with the C_3 coefficients obtained from perturbation theory. Note that singlet and triplet curves merge together before $R=30a_0$ and, therefore, for larger R values exchange interaction is negligible. This means that a perturbative approach as the one discussed in Sec. III that ignores exchange is in principle applicable beyond this internuclear distance. A quantitative comparison of the present nonperturbative results with the prediction of the perturbation theory is given in Table IV. An agreement within 8 to 9 significant digits is found. Note, the energies obtained with the present approach are mostly lower than the ones predicted by the perturbation theory. Extensive tests were performed to check the numerical stability of the nonperturbative calculations and their convergence with respect to the expansion length of the basis set. Since these tests indicate a numerical stability of 13 digits and a basis-set convergence within at least 9 significant digits for $R=80a_0$ and 11 digits for $200a_0$, the observed small remaining discrepancies are very likely to be caused by the higher-order terms omitted in the present perturbative expansion.

The correctness of the CI wave function itself can be checked by comparing the projection coefficients $U_{i\alpha}(R,\boldsymbol{\tau})$ with their asymptotes $U_{i\alpha}^{(0)}(R,\tau)$ obtained by means of the perturbative theory. An example is shown in Fig. 5 where the projection coefficients of the resonant wave functions $|\alpha^3\Sigma_u^+\rangle$ onto $|\{1\}^3\Sigma_u^+\rangle$ [asymptotically corresponding to the H($2s$) + H($2s$) collisional channel] are compared with their perturbatively calculated asymptotes $U_{1\alpha}^{(0)}(R,\Sigma_+^+)$. Excellent agreement is found for $R>30a_0$. The complicated behavior of $U_{1\alpha}(R,\Sigma_u^+)$ for $\alpha=3,4$ at small R is evidence for the existence of avoided crossings.

The significance and reliability of the new results can be demonstrated with the aid of a quantitative analysis of the $2\,^1\Pi_g$ and the $2\,^3\Pi_u$ states given in Fig. 6. Here the results of the CI calculations are compared with the old and the new perturbation-theory results. The inclusion of higher-order terms in the new asymptotic formula leads to significantly better agreement with the CI data. The new results differ very clearly from the earlier prediction of perturbation theory [5,13]. In fact, the character of the interaction changes from an attractive to a repulsive one.

A comparison of the energies of the $4\,^1\Sigma_g^+$ and $4\,^3\Sigma_u^+$ states with the asymptotic behavior predicted by perturbation theory is given in Fig. 7. The energies of the $Q(2)$ states are plotted as $(E+0.25)R^5+C_3R^2$ versus the inverse internuclear distance R^{-1} and thus should converge to the corresponding C_5 coefficient. This picture shows that not only the leading term of the van der Waals expansion can be extracted from the results of the CI calculations but it is also possible to make a good estimation of the second term. This can be seen as an additional proof of the reliability of the present results. The fact that it is possible to extract such information from CI calculations is especially impressive taking into account the very small quantitative contribution of the C_5 term to the

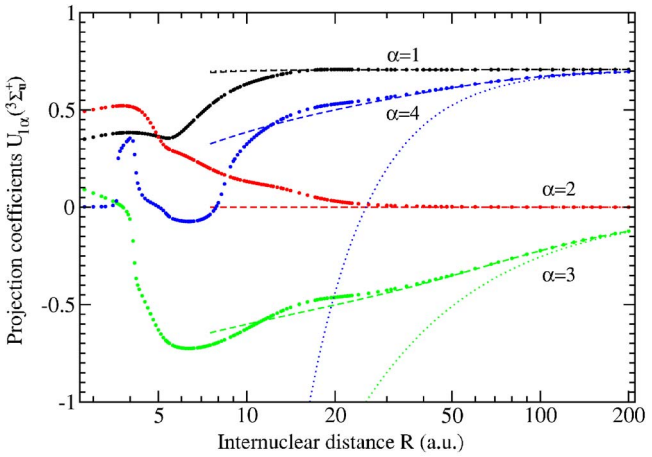

FIG. 5. (Color online) The projection coefficients $U_{1\alpha}(R,^3\Sigma_u^+)$ obtained with the nonperturbative CI calculation (circles) are compared with asymptotes given by the first-order perturbation theory. Dashed lines depict corresponding $U_{1\alpha}^{(0)}(R,\Sigma_+^+)$ functions whereas point lines depict the expansion (24) of $U_{1\alpha}^{(0)}(R,\Sigma_+^+)$ including only the first three terms.

energy (4×10^{-7} a.u. for $R=100a_0$ with a contribution of the C_3 term of about 2.2×10^{-5} a.u.)

For the use of the diabatic basis in subsequent scattering calculations it is important to analyze the measure of completeness $\Omega_\alpha(R,\tau)$. An example of such analysis is presented in Fig. 8 where functions $\Omega_\alpha(R,^3\Sigma_+^u)$ are given for the full range of internuclear distances R. The Ω_α converge for large R to 0 as (approximately) 10^5R^{-6} which can be explained as a contribution of all other diabatic states introduced via higher-order perturbations. Although the diabatic basis (25) with $|\{j\}\tau\rangle$ given by Eqs. (9)–(19) is complete within 1% for $R>20a_0$, it becomes clearly incomplete for small R (especially for the higher-lying resonances). Therefore, the diabatic basis should be used with caution in cases where the atoms come close to each other.

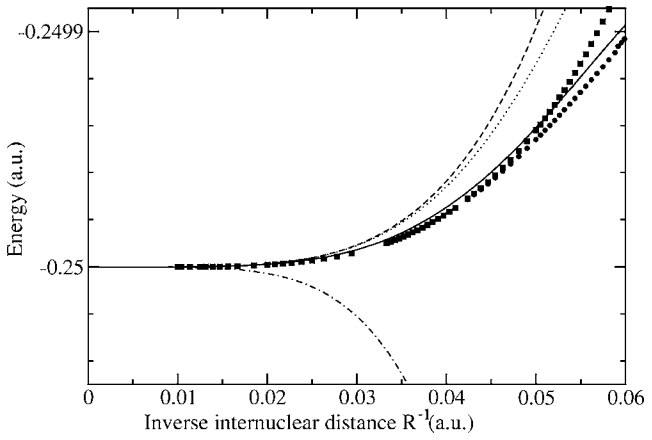

FIG. 6. Energy of 2 $^1\Pi_g$ state (squares) and 2 $^3\Pi_u$(circles) compared with their asymptotic behavior predicted by perturbation theory. The dashed line depicts the result of the first-order perturbation theory $E_2^{(1)}(R;\Pi_+)$, solid line depicts $E_2^{(1)}(R;\Pi_+)+\frac{C_{2;6}^{(2)}(\Pi_+)}{R^6}$. The chain line depicts $\frac{C_5}{R^5}$ with the previously erroneously calculated C_5 coefficient [5,13]. The dotted line depicts the leading terms of the expansion (23), i.e., $\frac{C_{2;5}^{(1)}(\Pi_+)}{R^5}+\frac{C_{2;7}^{(1)}(\Pi_+)}{R^7}$.

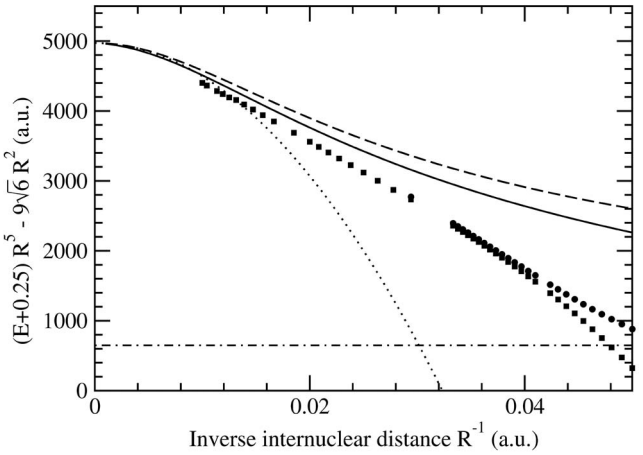

FIG. 7. Energies of the 4 $^1\Sigma_g^+$ (squares) and the 4 $^3\Sigma_u^+$ state (circles) compared with the asymptotic behavior predicted by perturbation theory. The dashed line is the result of first-order perturbation theory $E_4^{(1)}(R;\Sigma_+^+)$, the solid line is $E_4^{(1)}(R;\Sigma_+^+)+\frac{C_{4;6}^{(2)}(\Sigma_+^+)}{R^6}$. The chain line shows the prediction obtained with the previous erroneous C_5 coefficient. The dotted line depicts the leading terms of the expansion (23), i.e., $\frac{C_{4;3}^{(1)}(\Sigma_+^+)}{R^3}+\frac{C_{4;5}^{(1)}(\Sigma_+^+)}{R^5}+\frac{C_{4;7}^{(1)}(\Sigma_+^+)}{R^7}$.

An important point should be mentioned about the expansions (23) and (24) of $E_\alpha^{(1)}(R;\tau)$ and $U_{i\alpha}^{(0)}(R,\tau)$ obtained within the first-order perturbation theory. Note, the diagonalization of the coupling matrices in Eq. (20) for $\tau=\Sigma_+^+$, Π_+ provides rather complicated analytical formulas for $E_\alpha^{(1)}(R;\tau)$ and $U_{i\alpha}^{(0)}(R,\tau)$. Therefore, the expansions (23) and (24) appear to simplify the analysis. It is then tempting in pure first-order calculations to ignore, e.g., terms of order $R^{-7},R^{-9},\ldots$ in the expansion of the energy $E_\alpha^{(1)}(R;\tau)$ in Eq. (23), since the second-order perturbation theory provides terms of order R^{-6}. However, for some states convergence of the expansion (23) is extremely slow. In this case the neglect

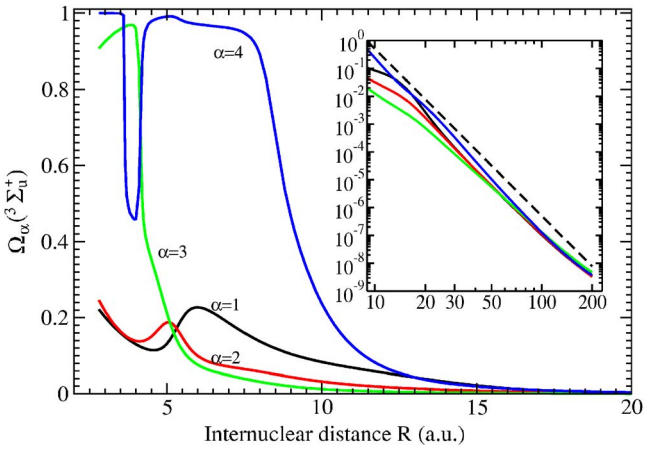

FIG. 8. (Color online) Measure of completeness $\Omega_\alpha(R,^3\Sigma_u^+)$ [defined in Eq. (26) for full range of internuclear distances]. The inset shows the long-range behavior on a logarithmic scale. The function $5\times10^5R^{-6}$ (dashed line) is given to guide the eye.

of higher-order terms in the expansion (23) leads for $R=30-60a_0$ to a much more severe error than the one due to the neglect of the contribution from higher-order perturbation theory, $E_\alpha^{(>1)}(R;\tau)=E_\alpha(R;\tau)-E_\alpha^{(1)}(R;\tau)$. Figure 7 shows the slow convergence of expansion (23) for the $|4\Sigma_+^+\rangle$ state. Although the omitted terms are proportional to larger powers of R^{-1} (namely, R^{-9}, R^{-11}, etc.) than the leading term of the second-order perturbation theory, R^{-6}, their contribution to the final result is much larger in the interval $R=30-60a_0$ and cannot be simply ignored. As shown in Fig. 5 the expansions (24) of $U_{1\alpha}^{(0)}(R,\Sigma_+^+)$ with only the first three terms being included leads for $\alpha=3,4$ to a significant deviation from the correct result already for $R<100a_0$, although the analytical formulas provide a satisfactory agreement down to $R=30a_0$. Therefore, the use of the expansions (23) and (24) should be done with some care, if internuclear distances $R<100a_0$ are of importance.

VI. SUMMARY

In this work all doubly excited $Q(2)$ states of H_2 converging asymptotically to the $H(n=2)+H(n'=2)$ limit have been calculated by means of a recently developed B-spline based CI method. A careful basis-set optimization was performed in order to yield converged results for internuclear separations in between 1 and $200a_0$. The present CI calculation is sufficiently accurate to achieve a connection between the short range and the asymptotic van der Waals regime. This removes the previous need for an interpolation that bridges these two extreme regimes and is very important for scattering calculations, especially in the case of low collision energies. For a large number of states the CI results agreed, for very large internuclear distances, very well with earlier predictions of first-order perturbation theory. However, in some cases the agreement was very unsatisfactory. This motivated a careful reanalysis of first-order perturbation theory including an extension to evaluate also the leading term (C_6) of second-order perturbation theory. It turned out that an erroneously invoked symmetry argument had led in the previous work [13] to the neglect of certain coupling terms. The newly derived van der Waals coefficients result is now in a very satisfactory agreement between the CI and the perturbative results for very large internuclear separations. It should, however, be noted that at the level of accuracy achieved in this work also relativistic and retardation effects start to become important.

Since scattering calculations describing atomic collision processes are usually performed in a diabatic representation, it is important to connect the results of a fully converged adiabatic molecular calculation to such diabatic states. A suitable diabatic basis is proposed for the description of $H(n=2)+H(n'=2)$ collisions. The matrix describing the projection of relevant $Q(2)$ states onto the diabatic basis was calculated and its asymptote was analyzed. This included a demonstration of its relation to a power-series expansion of the corresponding transformation matrix connecting the atomic states (used in deriving the van der Waals coefficients) and the adiabatic ones. A measure of completeness of the diabatic basis was also introduced and evaluated. This measure is based on a projection onto the fully converged adiabatic CI wave functions. In this way the calculated CI wave functions can also serve as a valuable tool for validating the use of some diabatic basis for scattering calculations describing $H(n=2)+H(n'=2)$ collisions, since the measure of completeness provides information about the range of internuclear separations for which a particular diabatic basis is sufficiently complete.

ACKNOWLEDGMENTS

A.S. and Y.V. acknowledge financial support by the *Deutsche Forschungsgemeinschaft* (DFG-Sa 936/1) within the SPP 1116. A.S. is grateful to the *Stifterverband für die Deutsche Wissenschaft* (Programme *Forschungsdozenturen*), the *Fonds der Chemischen Industrie* and the European COST Programme D26/0002/02 for financial support. A.D. was supported by the Chemical Sciences, Geosciences and Biosciences Division of the Office of Basic Energy Sciences, Office of Science, U.S. Department of Energy. R.C.F. acknowledges support from the NSF through Grant No. PHY-0244066 and PHY-0554794. R.C.F. and P.F. acknowledge the support from the NSF through a grant to ITAMP at Harvard University and Smithsonian Astrophysical Observatory. P.F. and S.J. acknowledge the support from the Swedish Research Council.

APPENDIX: COEFFICIENTS $A_{ij}(\tau)$

The exchange integrals $S_{ij}(R;\tau)\equiv\langle\{i\}\tau|\hat{\mathcal{P}}_{12}|\{j\}\tau\rangle$ can be calculated using two-center integrals over Slater orbitals

$$I_1 \equiv {}_A\langle 2s|2s\rangle_B = \left(1+\frac{R}{2}+\frac{R^2}{12}+\frac{R^4}{240}\right)e^{-R/2}; \tag{A1}$$

$$I_2 \equiv {}_A\langle 2s|2p^0\rangle_B = R^3\left(\frac{1}{120}+\frac{R}{240}\right)e^{-R/2}; \tag{A2}$$

$$I_3 \equiv {}_A\langle 2p^0|2p^0\rangle_B = = \left(1+\frac{R}{2}+\frac{R^2}{20}-\frac{R^3}{60}-\frac{R^4}{240}\right)e^{-R/2}; \tag{A3}$$

$$I_4 \equiv {}_A\langle 2p^\pm|2p^\pm\rangle_B = \left(1+\frac{R}{2}+\frac{R^2}{10}+\frac{R^3}{120}\right)e^{-R/2}; \tag{A4}$$

where the label A (B) specifies the proton to which the atomic orbital is attached.

Nonzero integrals $S_{ij}(R;\tau)=S_{ji}(R;\tau)$ are

$$\begin{aligned}
&S_{11}(R;\Sigma_+^+)=I_1^2; && S_{11}(R;\Sigma_-^+)=I_2^2+I_1I_3;\\
&S_{12}(R;\Sigma_+^+)=-I_2^2; && S_{11}(R;\Sigma_-^-)=-I_4^2;\\
&S_{13}(R;\Sigma_+^+)=\sqrt{2}I_1I_2; && S_{11}(R;\Pi_+)=-I_1I_4;\\
&S_{22}(R;\Sigma_+^+)=I_3^2; && S_{22}(R;\Pi_+)=I_3I_4;\\
&S_{23}(R;\Sigma_+^+)=\sqrt{2}I_2I_3; && S_{11}(R;\Pi_-)=-I_3I_4;\\
&S_{33}(R;\Sigma_+^+)=I_2^2-I_1I_3; && S_{22}(R;\Pi_-)=I_1I_4;\\
&S_{44}(R;\Sigma_+^+)=I_4^2; && S_{11}(R;\Delta_+)=I_4^2.
\end{aligned} \tag{A5}$$

Only the states $|\{i\}\Sigma_+^+\rangle$, $i=1,2,3$ are coupled with each other via the operator $\hat{\mathcal{P}}_{12}$. The functions $A_{ij}(R;\boldsymbol{\tau})$ for $\boldsymbol{\tau}=\{p_s,\Sigma_+^+\}$ and $i,j=1,2,3$ can be obtained using an orthonormalization procedure for the 3×3 coupling matrix

$$W=\begin{pmatrix} 1+p_sI_1^2 & -p_sI_2^2 & \sqrt{2}p_sI_1I_2 \\ -p_sI_2^2 & 1+p_sI_3^2 & \sqrt{2}p_sI_2I_3 \\ \sqrt{2}p_sI_1I_2 & \sqrt{2}p_sI_2I_3 & 1+p_s(I_2^2-I_1I_3) \end{pmatrix} \tag{A6}$$

leading to the following nonzero coefficients $A_{ij}(R;\{p_s,\Sigma_+^+\})\equiv\tilde{A}_{ij}$ for $i,j=1,2,3$

$$\tilde{A}_{11}=W_{11}^{-1/2}; \tag{A7}$$

$$\tilde{A}_{22}=(W_{22}-W_{12}^2/W_{11})^{-1/2}; \tag{A8}$$

$$\tilde{A}_{21}=-\tilde{A}_{22}W_{12}/W_{11}; \tag{A9}$$

$$\tilde{A}_{33}=\left(\frac{W_{11}(W_{22}W_{33}-W_{23}^2)-W_{13}^2W_{22}}{W_{11}W_{22}-W_{12}^2}+\frac{2W_{12}W_{13}W_{23}-W_{12}^2W_{33}}{W_{11}W_{22}-W_{12}^2}\right)^{-1/2}; \tag{A10}$$

$$\tilde{A}_{32}=-\tilde{A}_{33}\frac{W_{11}W_{23}-W_{12}W_{13}}{W_{11}W_{22}-W_{12}^2}; \tag{A11}$$

$$\tilde{A}_{31}=-\tilde{A}_{33}\frac{W_{13}}{W_{11}}-\tilde{A}_{32}\frac{W_{12}}{W_{11}}. \tag{A12}$$

The remaining coefficients $A_{ij}(R;\boldsymbol{\tau})$ are given by

$$A_{ij}(R;\boldsymbol{\tau})=\delta_{ij}[1+p_sS_{ii}(R;\tau)]^{-1/2}. \tag{A13}$$

[1] D. Zajfman, Z. Amitay, C. Broude, P. Forck, B. Seidel, M. Grieser, D. Habs, D. Schwalm, and A. Wolf, Phys. Rev. Lett. **75**, 814 (1995).

[2] C. Strömholm I. F. Schneider, G. Sundström, L. Carata, H. Danared, S. Datz, O. Dulieu, A. Källberg, M. af Ugglas, X. Urbain, V. Zengin, A. Suzor-Weiner, and M. Larsson, Phys. Rev. A **52**, R4320 (1995).

[3] F. Martín, J. Phys. B **32**, R197 (1999).

[4] N. Kolachevsky, M. Fischer, S. G. Karshenboim, and T. W. Hänsch, Phys. Rev. Lett. **92**, 033003 (2004).

[5] R. C. Forrey, S. Jonsell, A. Saenz, P. Froelich, and A. Dalgarno, Phys. Rev. A **67**, 040701(R) (2003).

[6] D. Landhuis, L. Matos, S. C. Moss, J. K. Steinberger, K. Vant, L. Willmann, T. J. Greytak, and D. Kleppner, Phys. Rev. A **67**, 022718 (2003).

[7] U. Fano, Phys. Rev. **124**, 1866 (1961).

[8] J. Tennyson, At. Data Nucl. Data Tables **64**, 253 (1996).

[9] S. Jonsell, A. Saenz, P. Froelich, R. C. Forrey, R. Cote, and A. Dalgarno, Phys. Rev. A **65**, 042501 (2002).

[10] S. L. Guberman, J. Chem. Phys. **78**, 1404 (1983).

[11] I. Sánchez and F. Martín, J. Chem. Phys. **110**, 6702 (1999).

[12] Y. V. Vanne and A. Saenz, J. Phys. B **37**, 4101 (2004).

[13] S. I. Nikitin, V. N. Ostrovskii, and N. V. Prudov, Sov. Phys. JETP **64**, 745 (1986); Note, the English translation includes several typos in the definition of the transformations. It should read $P_0:\mathbf{r}_{1a}\rightarrow-\mathbf{r}_{1a},\mathbf{r}_{2b}\rightarrow-\mathbf{r}_{2b}$; $P_1:\mathbf{r}_{1a}\rightarrow-\mathbf{r}_{1a},\mathbf{r}_{2b}\rightarrow\mathbf{r}_{2b}$.

[14] X. Urbain, A. Cornet, and J. Jureta, J. Phys. B **25**, L189 (1992).